Comprehensive anatomical and functional imaging in patients with type I neurofibromatosis using simultaneous FDG-PET/MRI

Poster No.:	C-0589
Congress:	ECR 2019
Type:	Scientific Exhibit
Authors:	C. P. Reinert, M. Schuhmann, B. Bender, C. La Fougère, J. Schäfer, S. Gatidis; Tübingen/DE
Keywords:	Hybrid Imaging, Oncology, Paediatric, PET-MR, MR, MR-Diffusion/ Perfusion, Molecular imaging, Staging, Neoplasia, Cancer
DOI:	10.26044/ecr2019/C-0589

Aims and objectives

The purpose of this study was to investigate the clinical use of combined FDG-PET/MRI in patients with NF1 for monitoring enlargement and metabolism of PNFs with regard to malignant transformation, as well as possibility to detect NF1 associated CNS lesions in standard T2 weighted brain images, which are part of the whole body PET/MRI standard protocol.

Methods and materials

This retrospective study was approved by our local institutional ethical review board and informed consent was waived (Project Number: 345/2018BO).

The underlying study population consisted of all patients with NF1 undergoing FDG-PET/MRI in our institution between September 2012 and February 2018 presenting with a clinical question referring to malignant transformation of known plexiform neurofibromas.

PET/MRI imaging

All combined PET/MRI examinations were performed on an integrated clinical PET/MRI system (Biograph mMR, Siemens Healthcare GmbH, Erlangen, Germany, software versions B20P and E11P) which is able to acquire PET and MRI simultaneously. For the generation of a segmentation-based PET attenuation correction map, a whole-body 3D T1-weighted spoiled gradient-echo sequence in end-expiratory breath-hold with Dixon-based fat-water separation was acquired. In patients newly examined after 01/2017 atlas-based bone-estimation was additionally available and performed for the purpose of attenuation correction. In all PET/MRI examinations the following MR measurements were performed: a transversal and coronal T2-weighted turbo spin echo (TSE) sequence, a coronal whole body short time inversion recovery (STIR) sequence in free breathing, whole body diffusion weighted imaging (DWI), whole body T1-weighted volumetric interpolated breath-hold examination (VIBE) sequence after intravenous injection of 0.1 mmol/kg gadolinium-based MRI contrast media (GADOVIST®), a fluid attenuated inversion recovery (FLAIR) sequence of the head as well as a contrast-enhanced T1-weighted 3D magnetization prepared rapid gradient echo (MPRAGE) sequence of the head.

Patients fasted for at least 6 hours before intravenous injection of [^{18}F] fluorodeoxyglucose (FDG). The recommended dose for whole body FDG-PET is weight-dependent and ranges between 3.5-7 MBq/kg for a 2-minute scan [16]. As the PET acquisition in PET/MRI is longer (4 min per bed in our case), we reduced these values by a factor of about 2 based on previous data [17]. The injected dose of ^{18}F-FDG patients received was adjusted to patient body weight (average: 2.5±0.60 MBq/kg). The corresponding effective doses of PET in pediatrics and adults were calculated from the applied activity, as described in a previous study [18]. PET acquisition was initiated 60 minutes after tracer injection.

The whole body scan was acquired over 6±2 bed positions. PET was reconstructed using a 3D ordered-subset expectation-maximization algorithm with 2 iterations, 21 subsets, matrix size 256 x 256, Gaussian filtering of 4 mm. The patient examination times were measured based on the acquisition time stamps that are documented in our Picture

Archiving Communication System (PACS) and included an interval of 10 minutes for repositioning patients in order to achieve whole body coverage, as the scan range was limited to 150 cm until the scanner was updated with an additional scanner coil in 2016.

Quantitative PNF lesion measurements

A maximum of six peripheral nerve target lesions were defined per patient. Of these, a maximum of four nerve target lesions per patient with visibly increased FDG uptake above blood pool levels and a maximum of two target lesions in similar anatomical localization and with similar size without visibly increased FDG uptake were selected. Entirely diffuse configurated plexiform neurofibromas without a definable geometry in MRI, typically infiltrating skin or muscle, were excluded from the evaluation. Image analysis was performed using the software SyngoVia (Siemens, Erlangen, Germany).

Lesion size was determined by measurement of the maximum axial diameter of each target lesion using the T1-weighted MRI sequence after intravenous contrast media application.

For all peripheral nerve lesions, PET quantification was performed measuring the mean, maximum and peak standardized uptake values ($SUV_{mean/max/peak}$) based on 50%-isocontour volumes of interests (VOIs). SUVmax is defined as the highest single-pixel value within a defined volume of interest (VOI), whereas SUVpeak is defined as an average SUV within a small, fixed-sized VOI (1 ml) centered on maximum-uptake part of the lesion [19]. For measuring the SUV_{mean} of reference tissues, we placed a 2 cm-diameter ROI in the right atrium (bloodpool) and a 5 cm-diameter ROI in the liver parenchyma. In all patients, lesion SUV_{mean}-to-liver SUV_{mean} ratios were calculated.

In MRI, we measured the mean and minimum apparent diffusion coefficients (ADC_{mean}; ADC_{min}) of all target lesions using circular regions of interest (ROI) with a radius comprising the whole of the lesion on the level of its largest transverse cross-section (large ROI analysis). Additionally, we applied small ROI measurements as previously described [20] in suspicions PNF parts with SUV_{mean} above 2 and MPNSTs by placing a ROI into the lesion area with the highest ^{18}F-FDG-uptake (small ROI analysis).

To assess the long-term development in size of all included PNF lesions, we measured the maximum axial lesion size also in available previous and follow-up PET/MRI or MRI examinations in which the same lesions were assessable (Fig.1). The growth rate was calculated by the quotient of axial diameter change from previous to follow-up examination and the time interval in months.

Qualitative radiological evaluation

For qualitative analysis, all image data were assessed by two radiologists in consensus. The morphological characteristics of all target lesions were categorized as target-like or not target-like. Target-like lesions were defined as centrally hypointense in T2-weighted images with a hyperintense rim resembling a target within PNF of peripheral nerves or large PNF accumulations in certain body areas. Contrast-medium enhanced target lesions were defined visually as clearly hyperintense lesions in T1-weighted images after intravenous MRI contrast medium injection.

Furthermore, we evaluated the presence of incidental areas of high signal intensity on T2-weighted FLAIR sequence in the white substance (white matter lesions), which are typical MR findings in the cerebellum, brainstem, basal ganglia and thalami [21]. Also, the presence of visible optic nerve gliomas was evaluated.

Reference standard

All specimens of resected lesions were histologically examined by our in-house pathology. For non-resected lesions, both the clinical course and imaging follow-up were used as clinical reference standard to characterize the lesion as benign or malignant. The surgical indication was based on a tumor board decision in which all individual cases were discussed.

Images for this section:

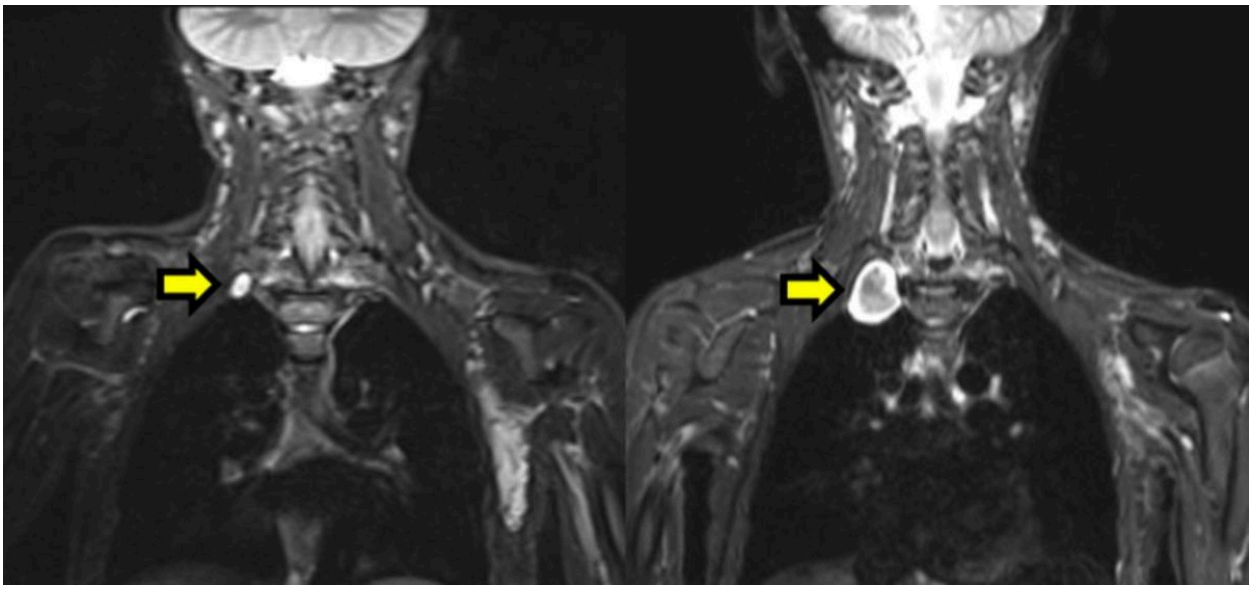

Fig. 1: 10-years-old NF1 patient with a PNF lesion in the right upper thoracic aperture in coronal STIR sequence showing significantly increasing size after 3 years of follow-up (left side: MRI only, performed 2013; right side: PET/MRI, performed 2016). In PET/MRI the measured MRI ADCmean of the lesion was 1779±180 x10#3mm2/s. The measured PET SUVmean was 2.9 (SUVmax 4.2). A MPNST has been proven after surgical resection with subsequent histopathological examination.

Results

28 patients [14 female; mean age 20 (2-44) years] with neurofibromatosis type 1 were included. 15 patients were children below the age of 18 years.

6/28 patients presented with one target lesion, 5/28 patients presented with two target lesions, 8/28 patients presented with three target lesions, 4/28 patients with four target lesions, 3/28 patients with five target lesions and 2/28 patients with six target lesions, respectively.

In the 28 patients cohort, 83 lesions were evaluated, of which 75 were rated as benign target lesions, 53/75 lesions were histologically examined after surgical resection and 22/75 lesions were not resected due to completely stable clinical course and imaging follow-ups (reference standard). In 6 patients 8 histologically proven MPNSTs were found, 5/6 patients had one MPNST and one patient had three MPNSTs.

PET/MRI imaging

23/83 target lesions were localized in the extremities, 25/83 target lesions were localized subcutaneously at the abdominal body trunk, intraabdominally or in the pelvis, 25/83 target lesions were localized thoracocervically and 10/83 target lesions were localized paravertebrally. Image examples of a benign target lesion and a MPNST are illustrated in Fig.2. The mean effective radiation dose patients received in our study was 3.24±1.65 mGy. The estimated mean examination time was 95±21 minutes per patient including five NF1 patients who had to be repositioned in order to achieve whole body coverage.

Quantitative PNF lesion measurements

The mean size of benign PNF lesions was 2.65±1.83cm, whereas the mean size of MPNSTs was 3.54±1.11cm (P<.01).

The measured PET SUV_{mean} of histologically proven MPNSTs was significantly higher than the SUV_{mean} of benign PNF lesions (3.84±3.98 [MPNSTs] vs. 1.85±1.03 [PNF]; P<.01) (Fig.3a). The SUV_{max} of histologically proven MPNSTs was similarly higher than the SUV_{max} of benign PNF (5.84±6.10 [MPNSTs] vs. 3.03±1.92 [PNF]; P<.01) (Fig.3b). Similarly, the lesion SUV_{mean}-to-liver SUV_{mean} ratio significantly differed between MPNSTs and PNF lesions (3.20±2.70 [MPNSTs] vs. 1.23±0.61 [PNF]; P<.01) (Fig.4). As significant cut-off values for differentiation between still benign PNF and MPNSTs we calculated SUV_{max} # 2.78 (sensitivity 0.88; specificity 0.73) and 1.45 for lesion SUVmean-to-liver SUVmean ratio (sensitivity 0.88; specificity 0.79).

MPNSTs showed only a tendency for higher diffusion restriction in large ROI analysis, which however did not reach statistical significance (ADC_{mean} values of benign PNF lesions and MPNSTs (1.87±0.24 $x10^{\#3}mm^2/s$ [PNF] vs. 1.76±0.11 $x10^{\#3}mm^2/s$ [MPNSTs]; P=1.0]. (Fig.5a). Similarly, small ROI analysis in lesion areas with the highest ^{18}F-FDG-uptake showed a tendency towards lower $ADC_{mean/min}$ values in MPNSTs compared to benign PNF with SUV_{mean} > 2 without statistical significance (P>.05) (Fig.5b).

24/28 patients had both a previous (mean time interval: 21.63±13.38 months) and follow-up (mean time interval: 13.26±7.94 months) PET/MRI or MRI examination. The estimated lesion growth rate correlated significantly with an increased glucose consumption as measured by means of PET SUV_{mean} (r_s=.41; P=.003) (Fig.6a), whereas no significant correlation was found between the lesion growth rate and the MRI ACD_{mean} in large ROI analysis (r_s=.07; P=.67) (Fig.6b).

25/75 benign PNF lesions presenting with a SUV_{mean} value below that of bloodpool SUV_{mean} (0.95±0.30) showed a significant lower growth rate per month than 50/75 benign PNF lesions with a relatively elevated SUV_{mean} value (-0.32±1.00%/month [SUVmean < bloodpool] vs. 1.10±2.25%/month [SUVmean > bloodpool]; P <.05) (Fig.7).

Qualitative radiological evaluation

49/75 benign PNF lesions and 6/8 MPNSTs showed an enhancement of contrast media, whereas 26/75 benign PNF lesions did not enhance (P=.50). 35/75 benign PNF lesions and 4/8 MPNSTs had a positive target sign (P=.86).

8/28 patients did not get an examination of the brain in PET/MRI because of an inconspicuous brain MRI examination performed shortly before the PET/MRI scan. The PET/MRI of 20/28 patients included a dedicated T2 weighted FLAIR brain protocol for screening purposes as described above. Out of these 20 patients, 14 patients (70%) had T2-hyperintense focal areas of signal intensity (FASI) in brain parenchyma. Further, we found changes compatible with optic nerve gliomas in 8 patients (40%) (Fig.8).

Images for this section:

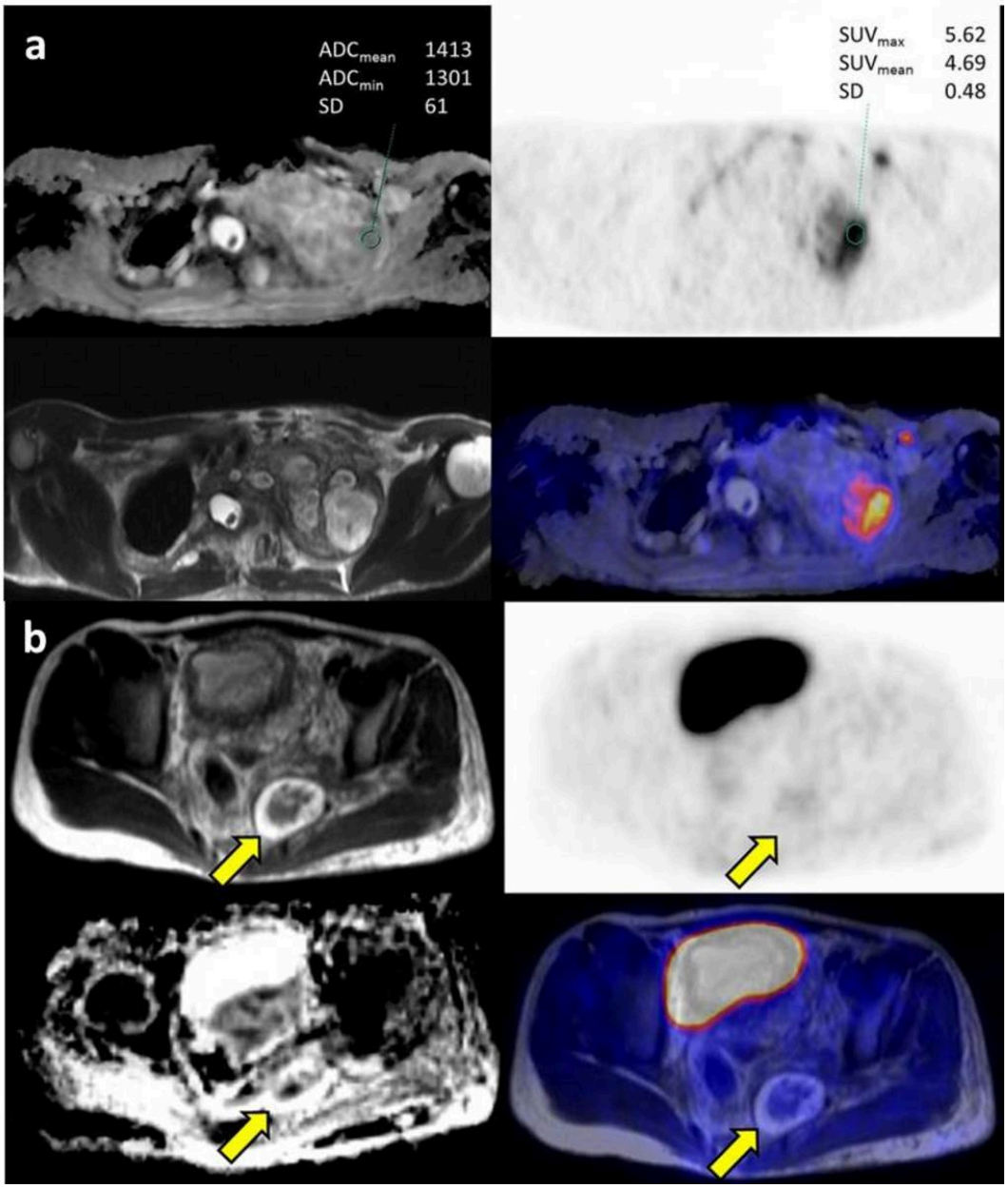

Fig. 2: A) 28-years-old NF1 patient with a MPNST in the left upper thoracic aperture located within a large PNF manifestation showing a heterogeneous diffusion restriction in ADC map (first row, left side). A small ROI was placed in the area with the most increased glucose metabolism in FDG-PET (first/second row, right side), copied and pasted in the ADC map for measurement. The second row on the left side shows the lesion in T2-weighted axial sequence. (B) 10-years-old NF1 patient with a benign PNF lesions in the left ischiorectal fossa showing a target-like configuration in T2-weighted axial sequences (fourth row, left side), a heterogeneous diffusion restriction in ADC map (third row, left side) and a glucose metabolism in FDG-PET below bloodpool SUV (third/fourth row, right side).

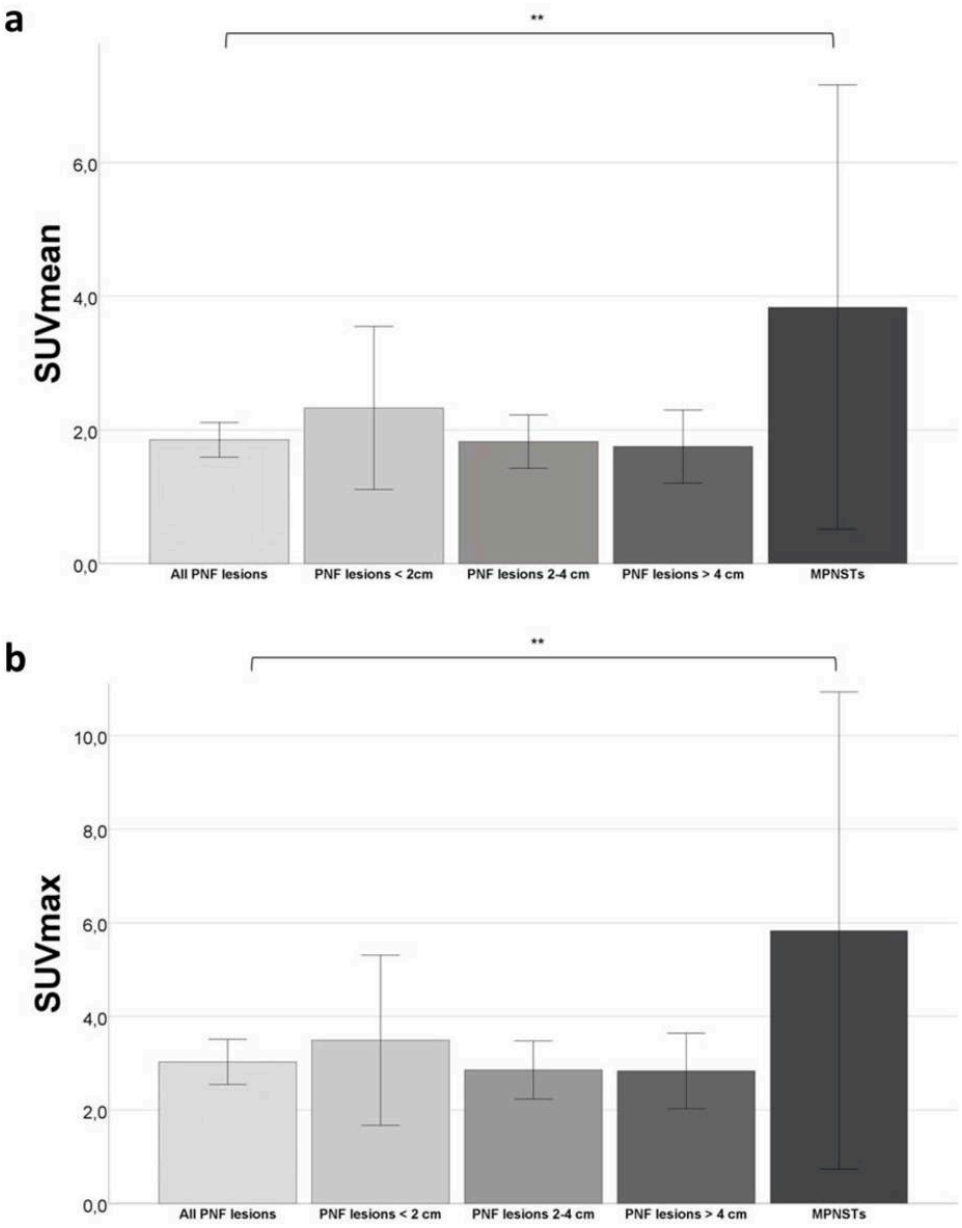

Fig. 3: (a) SUVmean ± 95% CI of all benign PNF lesions (n=75), lesions < 2cm in diameter (n=21), lesions 2-4 cm in diameter (n=30), lesions > 4cm in diameter (n=16) and MPNSTs (n=8). (b) SUVmax ± 95% CI of all benign PNF lesions (n=75), lesions < 2cm in diameter (n=21), lesions 2-4 cm in diameter (n=30), lesions > 4cm in diameter (n=16) and MPNSTs (n=8).

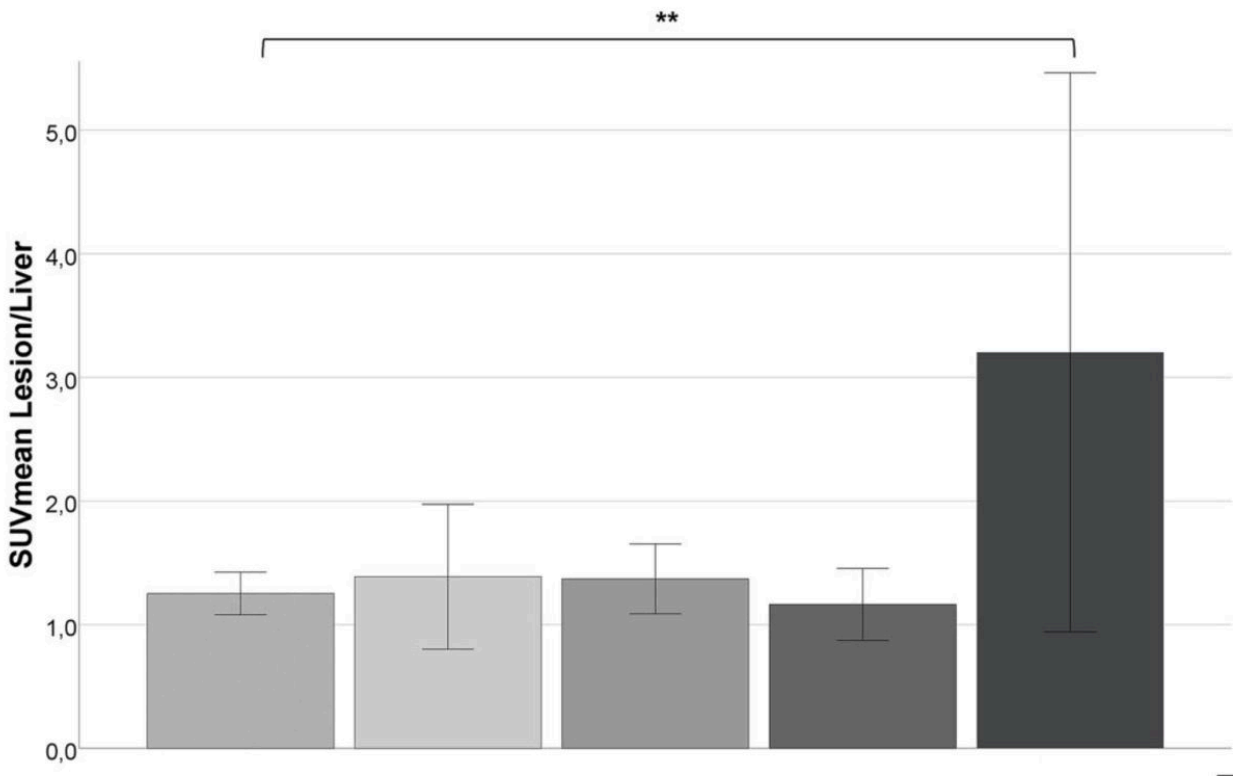

Fig. 4: Lesion SUVmean-to-liver SUVmean ratio ± 95% CI of all benign PNF lesions (n=75), lesions < 2cm in diameter (n=21), lesions 2-4 cm in diameter (n=30), lesions > 4cm in diameter (n=16) and MPNSTs (n=8).

© Reinert CP et al. (2018) Comprehensive anatomical and functional imaging in patients with type I neurofibromatosis using simultaneous FDG-PET/MRI. Eur J Nucl Med Mol Imaging [Epub ahead of print]

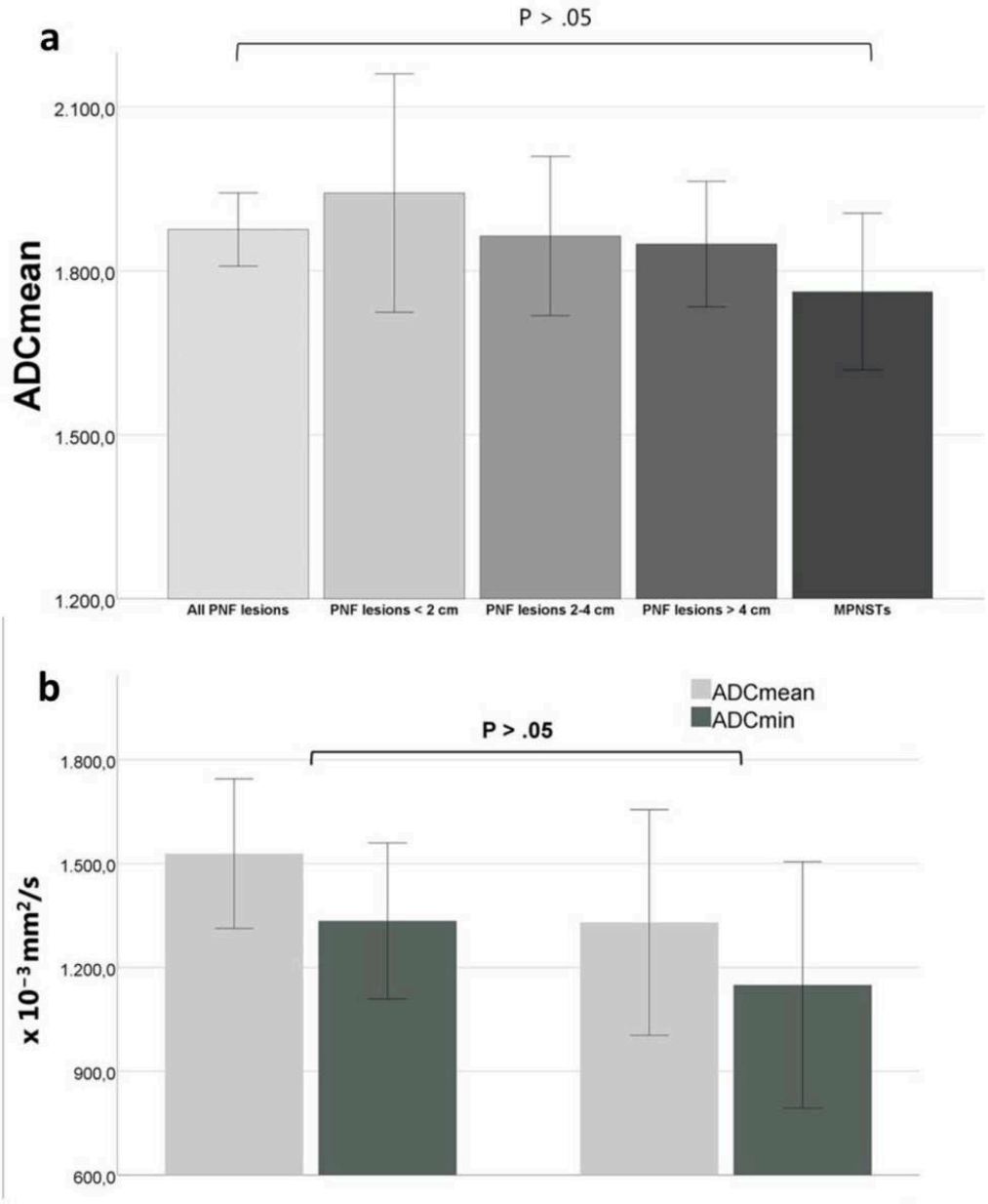

Fig. 5: (a) ADCmean ± 95% CI using large ROI analysis of all benign PNF lesions (n=75), lesions < 2cm in diameter (n=21), lesions 2-4 cm in diameter (n=30), lesions > 4cm in diameter (n=16) and MPNSTs (n=8). (b) ADCmean and ADCmin ± 95% CI using small ROI analysis of lesions with a measured SUVmean > 2 (n=13) and MPNSTs (n=8).

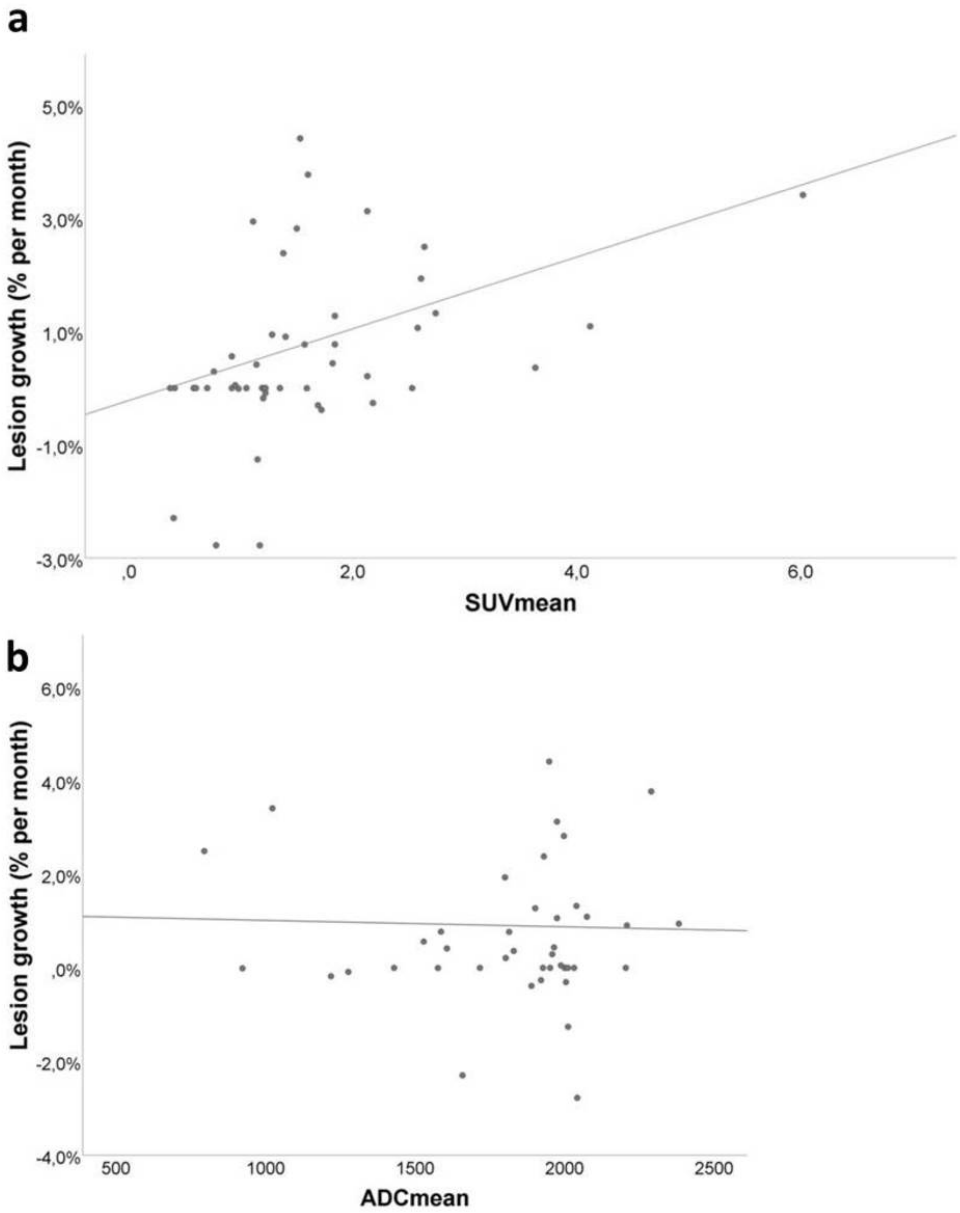

Fig. 6: (a) Bivariate correlation curve between the SUVmean and the lesion growth rate (percent per month) with a calculated Spearman's rank correlation coefficient rs=.4 and a P value of .003. (b) Bivariate correlation curve between the ADCmean using large ROI analysis and the lesions growth (percent per month) with a calculated Spearman's rank correlation coefficient rs=.07 and a P value of .67.

Fig. 7: Growth rate (percent per month) ± 95% CI in benign PNF lesions with a measured SUVmean < bloodpool (n=25) and in benign PNF lesions with a measured SUVmean > bloodpool (n=50).

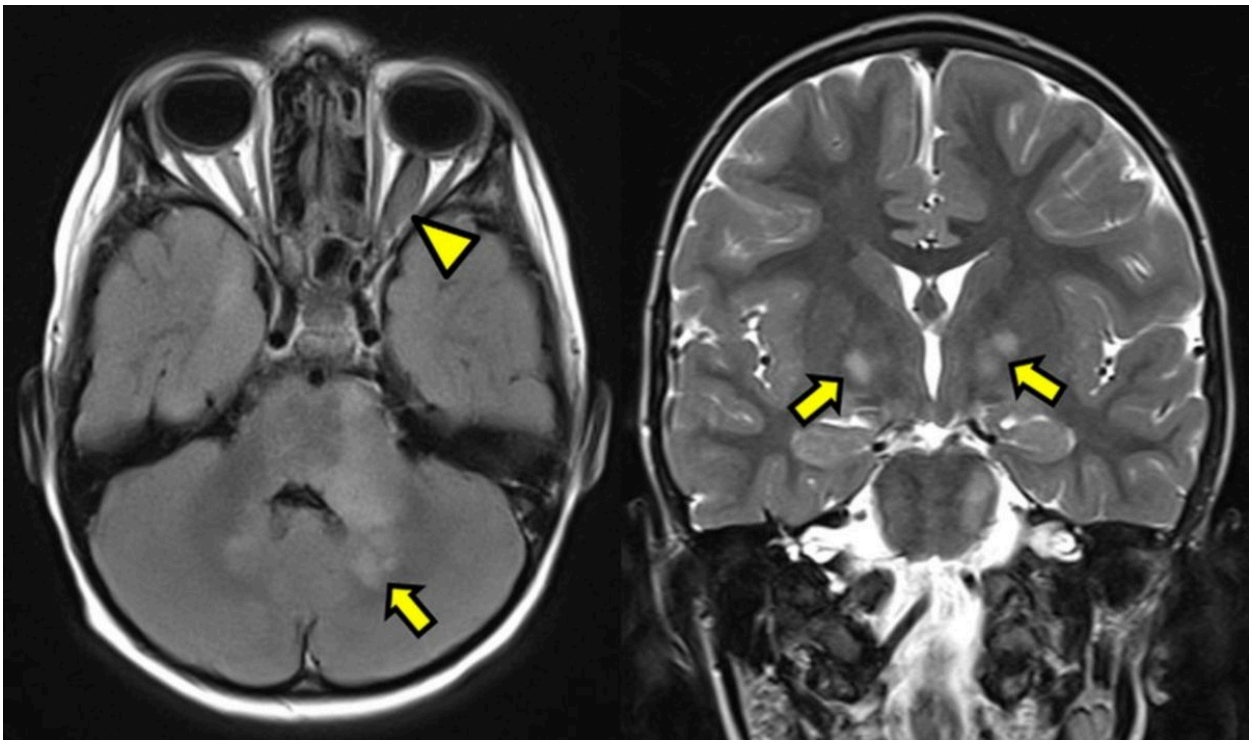

Fig. 8: Axial FLAIR-sequence (left side) and coronal T2-weighted TSE sequence of a 10-years-old NF1 patient with multiple T2-hyperintense focal areas of signal intensity (FASI) in the thalamic region of the brain (arrows) and a glioma of the left optic nerve (arrowhead).

Conclusion

Personal information

References

1. Yap, Y.S., et al., *The NF1 gene revisited - from bench to bedside.* Oncotarget, 2014. **5**(15): p. 5873-92.

2. Ferner, R.E., et al., *Guidelines for the diagnosis and management of individuals with neurofibromatosis 1.* J Med Genet, 2007. **44**(2): p. 81-8.

3. Ducatman, B.S., et al., *Malignant peripheral nerve sheath tumors. A clinicopathologic study of 120 cases.* Cancer, 1986. **57**(10): p. 2006-21.

4. Evans, D.G., et al., *Malignant peripheral nerve sheath tumours in neurofibromatosis 1.* J Med Genet, 2002. **39**(5): p. 311-4.

5. Combemale, P., et al., *Utility of 18F-FDG PET with a semi-quantitative index in the detection of sarcomatous transformation in patients with neurofibromatosis type 1.* PLoS One, 2014. **9**(2): p. e85954.

6. Canavese, F. and J.I. Krajbich, *Resection of plexiform neurofibromas in children with neurofibromatosis type 1.* J Pediatr Orthop, 2011. **31**(3): p. 303-11.

7. Wu, J.S. and M.G. Hochman, *Soft-Tissue Tumors and Tumorlike Lesions: A Systematic Imaging Approach.* Radiology, 2009. **253**(2): p. 297-316.

8. Piscitelli, O., et al., *Neurofibromatosis type 1 and cerebellar T2-hyperintensities: the relationship to cognitive functioning.* Dev Med Child Neurol, 2012. **54**(1): p. 49-51.

9. Gayre, G.S., et al., *Long-term visual outcome in patients with anterior visual pathway gliomas.* Journal of neuro-ophthalmology : the official journal of the North American Neuro-Ophthalmology Society, 2001. **21**(1): p. 1-7.

10. Omuro, A. and L.M. DeAngelis, *Glioblastoma and other malignant gliomas: A clinical review.* JAMA, 2013. **310**(17): p. 1842-1850.

11. Broski, S.M., et al., *Evaluation of 18F-FDG PET and MRI in differentiating benign and malignant peripheral nerve sheath tumors.* Skeletal Radiology, 2016. **45**(8): p. 1097-1105.

12. Demehri, S., et al., *Conventional and functional MR imaging of peripheral nerve sheath tumors: initial experience.* AJNR Am J Neuroradiol, 2014. **35**(8): p. 1615-20.

13. Gatidis, S., et al., *Comprehensive Oncologic Imaging in Infants and Preschool Children With Substantially Reduced Radiation Exposure Using Combined Simultaneous (1)(8)F-Fluorodeoxyglucose Positron Emission Tomography/Magnetic Resonance*

Imaging: A Direct Comparison to (1)(8)F-Fluorodeoxyglucose Positron Emission Tomography/Computed Tomography. Invest Radiol, 2016. **51**(1): p. 7-14.

14. Lu-Emerson, C. and S.R. Plotkin, *The Neurofibromatoses. Part 1: NF1.* Rev Neurol Dis, 2009. **6**(2): p. E47-53.

15. Chawla, S.C., et al., *Estimated cumulative radiation dose from PET/CT in children with malignancies: a 5-year retrospective review.* Pediatr Radiol, 2010. **40**(5): p. 681-6.

16. Boellaard, R., et al., *FDG PET/CT: EANM procedure guidelines for tumour imaging: version 2.0.* Eur J Nucl Med Mol Imaging, 2015. **42**(2): p. 328-54.

17. Schafer, J.F., et al., *Simultaneous whole-body PET/MR imaging in comparison to PET/CT in pediatric oncology: initial results.* Radiology, 2014. **273**(1): p. 220-31.

18. *Radiation dose to patients from radiopharmaceuticals (addendum 2 to ICRP publication 53).* Ann ICRP, 1998. **28**(3): p. 1-126.

19. Vanderhoek, M., S.B. Perlman, and R. Jeraj, *Impact of the definition of peak standardized uptake value on quantification of treatment response.* J Nucl Med, 2012. **53**(1): p. 4-11.

20. Neubauer, H., et al., *Diagnostic Value of Diffusion-Weighted MRI for Tumor Characterization, Differentiation and Monitoring in Pediatric Patients with Neuroblastic Tumors.* Rofo, 2017. **189**(7): p. 640-650.

21. Billiet, T., et al., *Characterizing the microstructural basis of "unidentified bright objects" in neurofibromatosis type 1: A combined in vivo multicomponent T2 relaxation and multi-shell diffusion MRI analysis.* Neuroimage Clin, 2014. **4**: p. 649-58.